

# Selective CO<sub>2</sub> Electrochemical Reduction Enabled by a Tricomponent Copolymer Modifier on a Copper Surface

Jianchun Wang, Tao Cheng, Aidan Q. Fenwick, Turki N. Baroud, Alonso Rosas-Hernández, Jeong Hoon Ko, Quan Gan, William A. Goddard III,\* and Robert H. Grubbs\*



Cite This: *J. Am. Chem. Soc.* 2021, 143, 2857–2865



Read Online

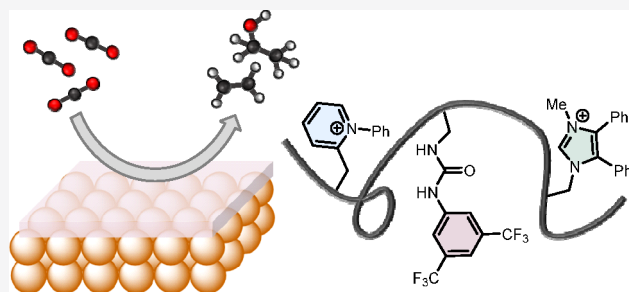
ACCESS |

Metrics & More

Article Recommendations

Supporting Information

**ABSTRACT:** Electrochemical CO<sub>2</sub> reduction over Cu could provide value-added multicarbon hydrocarbons and alcohols. Despite recent breakthroughs, it remains a significant challenge to design a catalytic system with high product selectivity. Here we demonstrate that a high selectivity of ethylene (55%) and C<sub>2+</sub> products (77%) could be achieved by a highly modular tricomponent copolymer modified Cu electrode, rivaling the best performance using other modified polycrystalline Cu foil catalysts. Such a copolymer can be conveniently prepared by a ring-opening metathesis polymerization, thereby offering a new degree of freedom for tuning the selectivity. Control experiments indicate all three components are essential for the selectivity enhancement. A surface characterization showed that the incorporation of a phenylpyridinium component increased the film robustness against delamination. It was also shown that its superior performance is not due to a morphology change of the Cu underneath. Molecular dynamics (MD) simulations indicate that a combination of increased local CO<sub>2</sub> concentration, increased porosity for gas diffusion, and the local electric field effect together contribute to the increased ethylene and C<sub>2+</sub> product selectivity.



## INTRODUCTION

Accumulation of the greenhouse gas CO<sub>2</sub> in the atmosphere due to excessive fossil fuel burning is the leading cause of today's climate change. Tremendous academic attention has therefore been directed toward the electrochemical CO<sub>2</sub> reduction (CO<sub>2</sub>RR), which is regarded as a promising scalable approach to convert CO<sub>2</sub> into valuable fuels or chemical feedstocks via solar- or wind-generated electricity.<sup>1</sup> Heterogeneous Cu catalysts have enjoyed unique reactivities toward multicarbon products due to their intermediate adsorption energy with CO; however, a total of 16 different products were observed.<sup>2</sup> Among these products, ethylene is particularly interesting, since it is in high industrial demand and provides an entry for many other feedstock chemicals through catalytic processes. Extensive investigations revealed that grain boundaries,<sup>3</sup> oxidation state,<sup>4</sup> dopants,<sup>5</sup> facets,<sup>6</sup> and morphology<sup>7</sup> could improve the catalytic activity and/or selectivity. However, the intrinsic CO<sub>2</sub>RR activity normalized by the electrochemical surface area of these nanostructured Cu catalysts has only marginally improved against a polycrystalline Cu foil surface thus far, whereas the surface roughness plays a vital role in determining the selectivity by modulating the local pH or mass transport.<sup>1a</sup> These studies highlight the difficulty of enriching the active sites on the surface while maintaining their structural stability.<sup>8</sup>

On the other hand, homogeneous molecular catalysts employ well-defined transition-metal complexes, in which the electronic and steric environment could be finely tuned by modifying the ligands.<sup>9</sup> Notably, leveraging noncovalent interactions by incorporating various functional groups into the secondary coordination sphere proved to be a viable approach to improve the catalytic properties of the molecular catalysts.<sup>10</sup> There has been a longstanding interest in borrowing concepts from these molecular catalysts to obtain heterogeneous catalysts.<sup>11</sup> Various molecular modifiers have been shown to tune the CO<sub>2</sub>RR selectivity by changing the electronic property of the metal via covalent bonding or altering the energy of adsorbates via noncovalent interactions.<sup>12</sup> In addition, some modifiers were shown to limit proton availability<sup>13</sup> or induce a morphology change<sup>14</sup> of the metal surface. As most of these molecular modifiers were small molecules with limited modularity of their structures, we strived to develop a family of copolymers that are both

Received: November 30, 2020

Published: February 11, 2021



modular and multifunctional so that a structure–activity relationship can be identified (Figure 1).

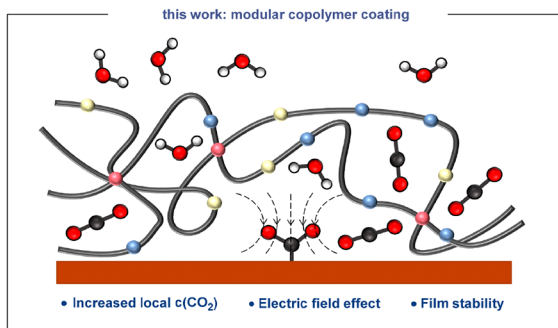


**Figure 1.** Tuning CO<sub>2</sub>RR product distribution using copolymer modifiers.

Ring-opening metathesis polymerization (ROMP) is a powerful and general method for synthesizing functionalized macromolecular materials.<sup>15</sup> The development of well-defined ruthenium metathesis catalysts has dramatically enhanced the functional group tolerance, allowing us the freedom to incorporate different types of functional groups. Unlike small-molecule modifiers, polymers are versatile in enhancing the selectivity for the CO<sub>2</sub>RR, because they not only allow the incorporation of functional groups in the side chain for noncovalent interactions but also naturally provide a hydrophobic environment that can regulate the local concentration of CO<sub>2</sub> and H<sub>2</sub>O.<sup>16</sup> Furthermore, the porosity of polymers can control the access of the reactants and minimize blockage of active sites on a heterogeneous surface. Our design principle is as follows. First, the polymer should create a hydrophobic environment that permits CO<sub>2</sub> gas transport while limiting the proton accessibility. Second, introduced functional groups will have noncovalent interactions with the adsorbed intermediates and/or water. Third, the polymer should remain stable on the electrode surface during the electrocatalysis.

## RESULTS AND DISCUSSION

**Electrochemical CO<sub>2</sub> Reduction Results.** At the beginning of this research, the effect of homopolymers with cationic side chains as modifiers was studied. It has been well documented that inorganic or organic cations would influence the productivity and selectivity of the CO<sub>2</sub>RR on the Cu electrode, primarily due to the electrostatic field stabilization of the adsorbates (e.g., \*OCCO).<sup>17</sup> Since the initial report<sup>18</sup> showing that ionic liquids could enhance the CO<sub>2</sub> to CO selectivity at a low overpotential on a Ag electrode, it has been hypothesized that ionic liquids might stabilize CO<sub>2</sub>RR intermediates through electrostatic interactions with adsorbates.<sup>19</sup> Inspired by these results, we decided to test a series of poly(ionic liquids) (PILs) on the Cu electrode. Bulk electrolysis experiments were performed on a polycrystalline copper electrode with CO<sub>2</sub>-saturated 0.1 M KHCO<sub>3</sub> electrolyte at pH 6.8. As shown in Figure 2, in the absence of modifiers and at a potential of  $-1.08\text{ V}_{\text{RHE}}$ , the pristine Cu electrode primarily produces hydrogen and methane, along with a relatively low production of C<sub>2+</sub> products, consistent with previous report<sup>2c</sup> (FE<sub>H2</sub> = 40%, FE<sub>CH4</sub> = 26%, FE<sub>C2H4</sub> = 22%). We then employed polymer 1 as the surface modifier, which can be viewed as a polymeric version of 1-butyl-3-methylimidazolium (BMIm). Polymer modifiers were spin-

coated onto the electropolished polycrystalline copper electrode. To our disappointment, using polymer 1 only affords hydrogen gas as the major product. It has been shown that hydrophilic modifiers will weaken the metal–hydride bond, thus yielding more H<sub>2</sub>.<sup>12h</sup> In addition, the strong polymer–metal interaction might block the access of CO<sub>2</sub> to the surface, thereby only affording H<sub>2</sub> (*vide infra*).

As an advantage of using organic modifiers, their chemical structures can be easily altered as desired. Systematic substitution of the imidazolium's C–H bonds by phenyl groups increased its hydrophobicity (polymers 2–4, see Figure S8 in the Supporting Information for their contact angles). The introduced phenyl substituents might also weaken intra- or intermolecular ion-pairing interactions so that the polymer layer might be more permeable to gas diffusion. In addition, substituents on imidazolium are also expected to increase its stability under alkaline conditions.<sup>19c,20</sup> We were delighted to find that the HER was indeed suppressed. Still, even the best polymer, 3, only offered an ethylene selectivity (FE<sub>C2H4</sub> = 22%) comparable to that of the unmodified Cu surface.

In addition to the electrostatic interaction of cations, hydrogen-bonding interactions might also help stabilize the intermediates of interest.<sup>12i</sup> Among the potential candidates for hydrogen-bonding donors, urea<sup>21</sup> and thiourea<sup>22</sup> have previously been utilized to enhance the performance of molecular catalysts. The direct use of poly-urea 5 led to only a marginal improvement. Interestingly, the random copolymer 6 consisting of both urea and imidazolium moieties improved the Faradaic efficiency for C<sub>2</sub>H<sub>4</sub> and inhibited the CH<sub>4</sub> production pathway, especially at the beginning of electrocatalysis. However, the CH<sub>4</sub>/C<sub>2</sub>H<sub>4</sub> ratio increased over time during the bulk electrocatalysis (Figure 3), implying the poor stability of the Cu/copolymer interface under electrocatalysis conditions (*vide infra*).

To improve the stability of the copolymer, we sought to incorporate a third monomer component. Inspired by the elegant work from the Agapie and Peters groups,<sup>12f,g,14</sup> we hypothesized that a small fraction of the phenylpyridinium moiety might have a stronger interaction with the Cu surface or act as a cross-linker upon electroreduction. Indeed, random copolymer 7 exhibited a stable electrocatalytic behavior (Figure 3), which led to a significant boost in the ethylene selectivity (FE<sub>C2H4</sub> = 50%). Further modification of the linker length between urea and the backbone slightly improved the FE<sub>C2H4</sub> value to 55% and the FE<sub>C<sub>2</sub></sub> value to 77% with random copolymer 8. To our knowledge, this rivals the highest Faradaic efficiencies for ethylene and C<sub>2+</sub> production using other modified polycrystalline Cu foil catalysts.

Control experiments were conducted to elucidate the structure–activity relationship. Changing the electron-withdrawing 3,5-bis(trifluoromethyl)phenyl group to a cyclohexyl group (random copolymer 10) led to a decrease in the ethylene production (FE<sub>C2H4</sub> = 37%), indicating that the chemical property of urea plays an important role in determining the product distribution. To prove that all three components in the copolymers 7–9 are essential, we tested the random copolymer 11 containing only imidazolium and pyridinium as well as the random copolymer 12 containing only urea and pyridinium. The catalytic behaviors of 11- and 12-modified Cu are similar to those the homopolymer 3- and 5-modified Cu, respectively. Therefore, the possibility that the selectivity enhancement was solely due to the presence of a

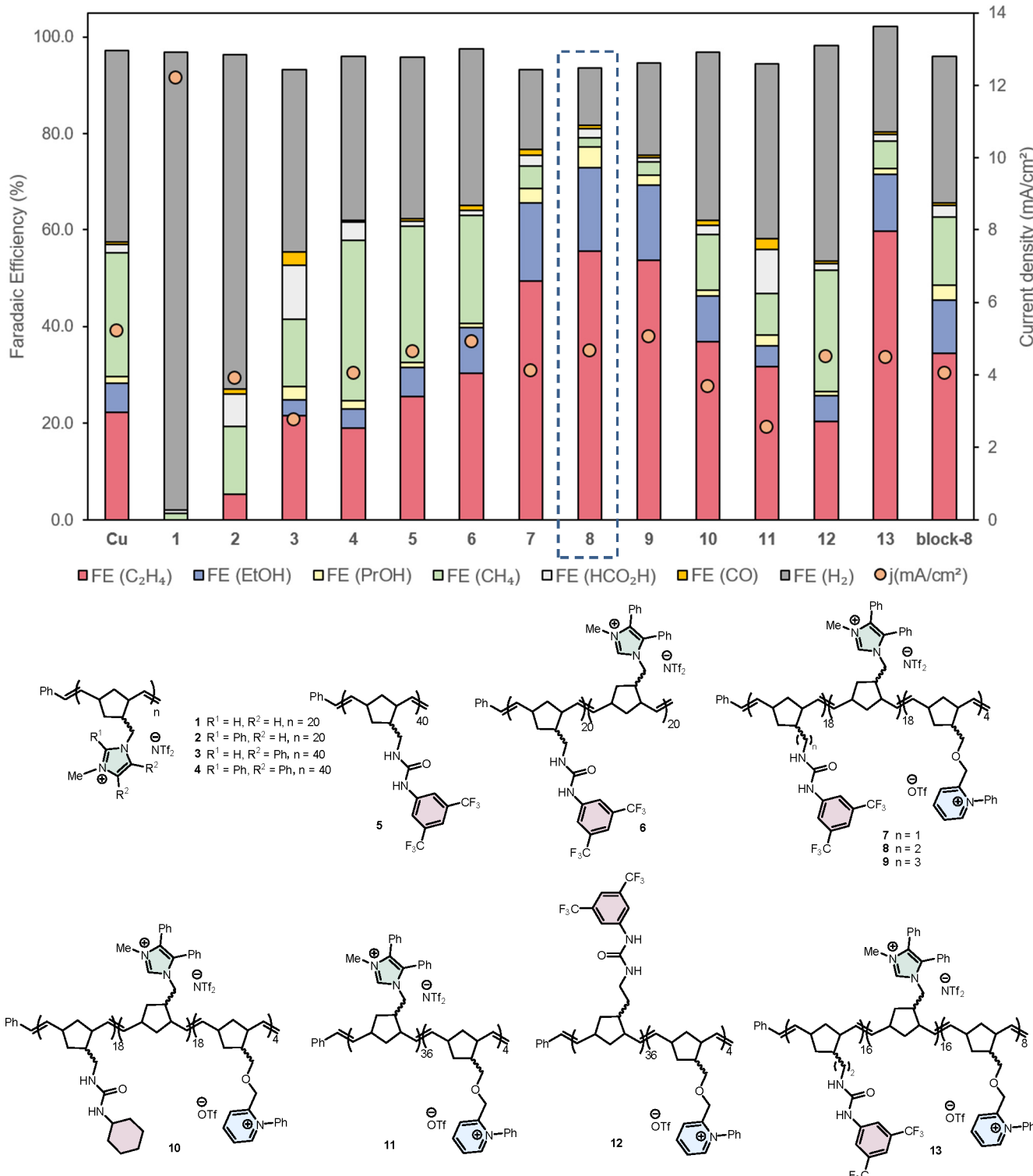


**Figure 2.** Faradaic efficiencies and current densities toward different products produced during  $\text{CO}_2$  reduction on polymer-modified polycrystalline copper electrodes. All copolymers were random copolymers unless noted otherwise. Electrocatalysis was conducted in  $\text{CO}_2$ -saturated 0.1 M  $\text{KHCO}_3$  at an applied potential of  $-1.08 \text{ V}_{\text{RHE}}$  for 64 min, unless noted otherwise. The experiment with polymer 1 modified Cu was conducted at  $-1.04 \text{ V}_{\text{RHE}}$ . Each data point shows the average of at least two individual measurements.

phenylpyridinium component was ruled out. An increase in the pyridinium ratio (random copolymer 13) resulted in a similar product distribution. Interestingly, the enhancement depends on not only the presence of all three components but also the sequence of the copolymer. In comparison with the random copolymer 8, the block copolymer block-8 gave inferior

Faradaic efficiencies for ethylene and  $\text{C}_{\geq 2}$  products (*vide infra* for discussion).

The products of the cathodic reaction using random copolymer 8 were analyzed at five different potentials. At a more positive potential ( $-0.90 \text{ V}$ ), hydrogen evolution became more competitive while a more significant portion of CO was

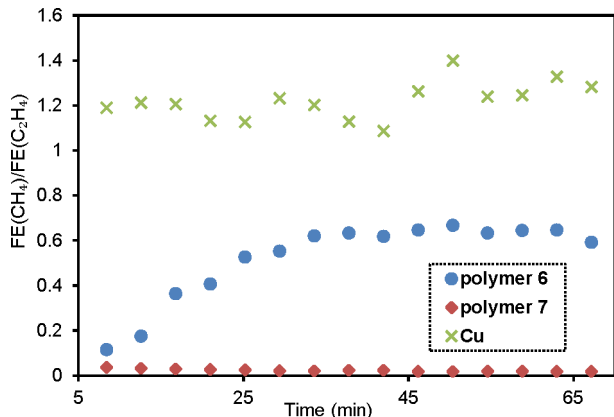


**Figure 3.** Stability in the Faradaic efficiencies of  $\text{CH}_4$  over  $\text{C}_2\text{H}_4$  using different copolymers.

produced (Figure 4), indicating that a more negative potential bias is needed to overcome the CO dimerization barrier. At a

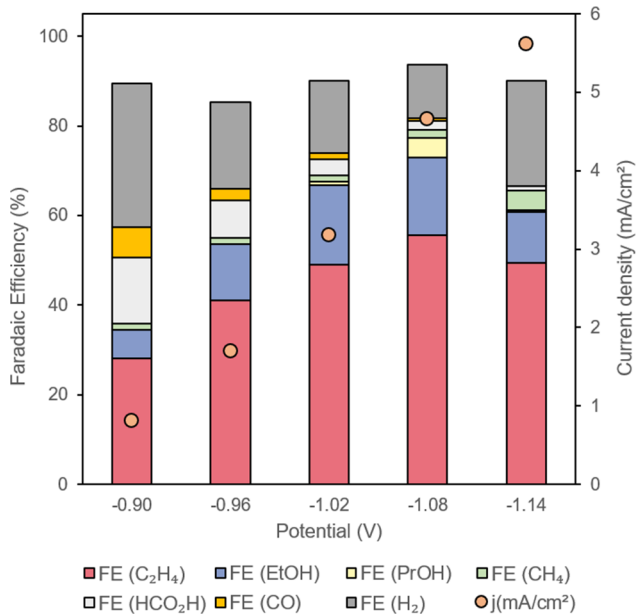


**Figure 4.** Faradaic efficiencies and current densities for  $\text{CO}_2\text{RR}$  products and hydrogen as a function of potential using the random copolymer 8 as the surface modifier. Each data point shows the average of two individual measurements.

more negative potential ( $-1.14 \text{ V}$ ), the Faradaic efficiency for ethylene decreases with an increase in the hydrogen evolution reaction. A Tafel analysis of ethylene production from  $\text{CO}_2$  gave a slope of  $142 \text{ mV/dec}$  (see Figure S1 in the Supporting Information), which is expected for the rate-limiting single-electron transfer to the adsorbed  $^{*}\text{CO}$  intermediate.

**Surface Characterization.** To investigate the effect of the phenylpyridinium side chain in stabilizing the polymer/metal interface, we performed *ex situ* scanning electron microscopy (SEM) experiments. The polymer 6 modified Cu electrode surface showed delamination of the polymer film after electrocatalysis, possibly due to gas production (Figure 5a–c). In sharp contrast, the mechanical stability of polymer 8 was significantly improved after incorporating the phenylpyridinium component. Significantly less delamination was observed after electrocatalysis (Figure 5d–f), showing improved robust-

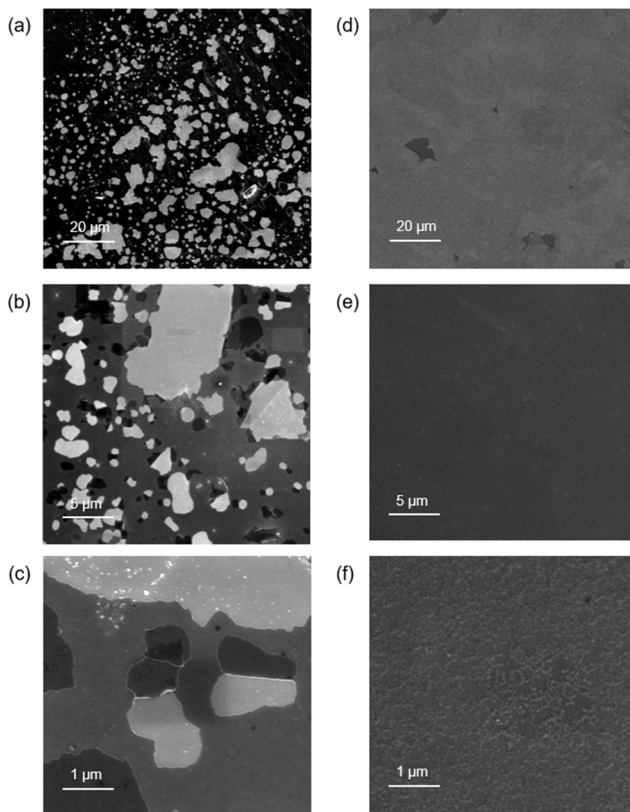


**Figure 5.** *Ex situ* SEM images of the Cu-foil electrode after electrocatalysis with different magnification ratios: (a–c) modified with random copolymer 6; (d–f) modified with random copolymer 8.

ness against gas evolution. At a higher magnification, a porous polymer surface was observed (Figure 5f). To further confirm that the surface observed in the SEM study is not the underlying Cu, an X-ray photoelectron spectroscopy (XPS) study of the same surface was conducted. The XPS survey spectra only showed the signals of the elements in the polymer rather than those of Cu. This result indicates that the surface was covered with the polymer film and that the thickness of the polymer film exceeds the depth of XPS analysis (see Figure S5 in the Supporting Information).

To gain more information about the change in surface morphology, we obtained atomic force microscopic (AFM) images before and after electrocatalysis. For the electropolished Cu without the polymer modifier, a smooth and flat surface was observed before electrocatalysis, with a root-mean-square roughness ( $R_q$ ) of  $1.9 \text{ nm}$  (Figure 6a). After the  $\text{CO}_2\text{RR}$  experiment was performed, the morphology of the pristine Cu electrode changed to a rougher surface ( $R_q = 13.8 \text{ nm}$ ) (Figure 6b), consistent with previous reports.<sup>14</sup> The AFM image of the polymer 8 modified Cu electrode showed a rough surface ( $R_q = 12.9 \text{ nm}$ ). After electrocatalysis, the surface roughness remained largely unchanged ( $R_q = 13.0 \text{ nm}$ ), consistent with the SEM results. On the other hand, the morphology of the underlying Cu surface might be important in controlling the electrocatalytic selectivity.<sup>23</sup> Some additives such as halide anions were reported to facilitate the nanostructuring process of Cu.<sup>6a,14</sup> To rule out this nanostructuring effect, we dissolved away the polymer film with organic solvents, and a smooth Cu surface ( $R_q = 2.8 \text{ nm}$ ) was observed by AFM (see Figure S4 in the Supporting Information). A further SEM study was consistent with the AFM results, and a SEM energy dispersive

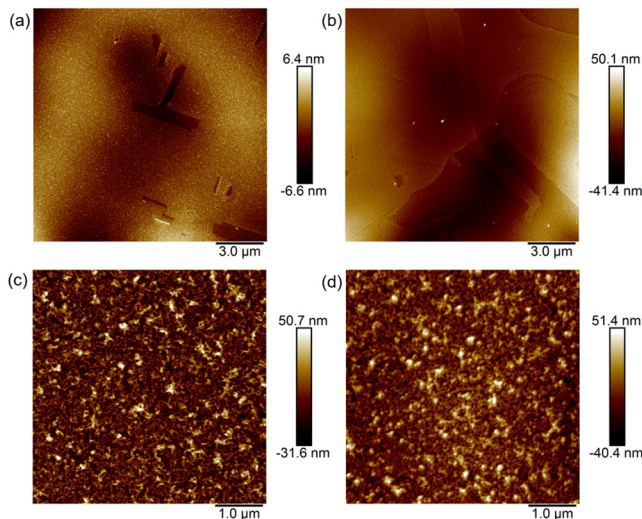


**Figure 6.** *Ex situ* AFM images of the Cu electrode: (a) unmodified, before electrocatalysis; (b) unmodified, after 64 min of electrocatalysis at  $-1.08\text{ V}$ ; (c) modified with random copolymer 8, before electrocatalysis; (d) modified with random copolymer 8, after 64 min of electrocatalysis at  $-1.08\text{ V}$ .

X-ray (EDX) analysis confirmed that the smooth surface was mainly comprised of Cu. These results confirmed that the enhancement in the ethylene and  $\text{C}_{2+}$  production was not caused by the formation of nanostructured Cu.

The thickness of the polymer layer was further investigated by AFM (**Figure 7**). A thin film of Cu was vapor-deposited on

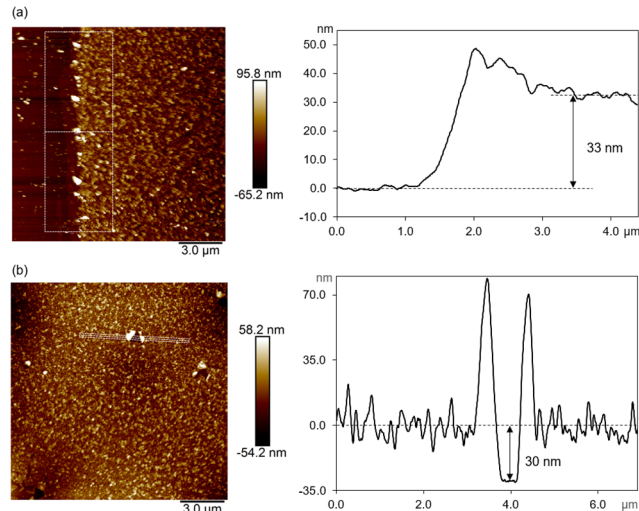


**Figure 7.** Thickness measurement using *ex situ* AFM images: (a) polymer-modified vapor-deposited Cu film with a scratch made by a razor blade; (b) Cu-foil electrode coated with random copolymer 8, after 64 min of electrocatalysis.

a silicon wafer and then was spin-coated with polymer 8. A portion of the polymer film was then removed with a razor blade. For an accurate measurement of polymer film thickness, the polymer film must be removed entirely in this region while at the same time the Cu surface underneath is not disturbed. First, the newly exposed region was scanned by the AFM probe tip to verify that only very little, if any, polymer material was left (see **Figure S3** in the Supporting Information). Second, a fresh vapor-deposited Cu film was scratched with the razor,

and no damage was visible under the experimental conditions. As shown in **Figure 7a**, the darker region corresponds to the exposed Cu surface, whereas the brighter region represents the polymer film. The white rectangular box is where the average cross-section was taken, from which the step height was calculated to be 33 nm. On the other hand, the film thickness can also be inferred from the AFM image of the post-electrocatalysis surface of the Cu electrode modified with copolymer 8. While the majority of the surface is robust during electrocatalysis, small portions of the film delamination were observable in the AFM image (**Figure 7b**). A cross-sectional analysis was taken across the exposed region, and the film thickness was estimated to be 30 nm.

**Proposed Mechanism for the Selectivity Enhancement.** Due to the complex structure of the polymers, it is difficult to deduce the information on the surface structure by only chemical intuition. In order to provide structural information on the electrode surface on the atomic scale, we carried out a multiscale simulation to directly study the interface structure. The atomistic scale molecular dynamics (MD) simulations reveal that polymers can increase the surface concentration of  $\text{CO}_2$ . We expect that a high  $\text{CO}_2$  concentration in the inner Helmholtz plane (IHP) should help  $\text{C}_{2+}$  production as well as suppress the HER,<sup>24</sup> whereas a low  $\text{CO}_2$  concentration would not. This effect is very dependent on the structure of the polymer, but there has been no atomistic explanation to guide the development of improved polymers. To help understand these phenomena, we carried out MD simulations, including a polymer with the same degree of polymerization in the experiment on a Cu (111) surface with sufficient  $\text{CO}_2$  and  $\text{H}_2\text{O}$  to extend the system to 6 nm, which consists of a Cu electrode (1 nm), a polymer–water mixture (4 nm), and water (1 nm) (see **Figure S10** in the Supporting Information). These calculations used the universal force field (UFF),<sup>25</sup> after revising to reproduce the interaction of polymer fragments with the Cu surface from density functional theory (DFT) calculations. The MD simulation is briefly summarized as follows, and more details are given in **Supporting Information**. First, we carried out MD with just the polymer and Cu surface for 2 ns. After that,  $\text{CO}_2$  and  $\text{H}_2\text{O}$  were introduced, followed by another 10 ns simulation. After this 12 (2 + 10) ns simulation, the potential energy is well converged, as are the geometries, indicating equilibrium of the MD (see **Figure S12** in the Supporting Information). A final 1 ns simulation was then carried out for analysis. The snapshots from MD simulations of water/Cu and random copolymer 8 + water/Cu are shown in **Figure 8a,b**. The presence of  $\text{CO}_2$  molecules within 5 Å from the surface, highlighted in **Figure 8a,b**, is the most relevant for the electrochemical reactions in the IHP. With 5 Å from the surface taken as a cutoff, the final 1 ns of MD trajectories shows that, for random copolymer 8, the average amount of  $\text{CO}_2$  at the water/Cu interface is  $0.86 \pm 0.04/\text{nm}^2$  in comparison to  $0.26 \pm 0.04$  for polymer 3 and  $0.36 \pm 0.05/\text{nm}^2$  for the case with no polymer (**Figure 8c**). We consider that this 2.4 times increase in  $\text{CO}_2$  at the Cu surface could explain why random copolymer 8 leads to 77% FE for  $\text{C}_{2+}$  products in comparison to 25% for polymer 3 (**Figure 2**). Interestingly, we noticed a linear correlation between the local  $\text{CO}_2$  concentration and the  $\text{CO}_2$  reduction performance using different polymers (see **Figure S14** in the Supporting Information), which might deserve a detailed investigation in the future. Moreover, the presence of the hydrophobic polymers limits the surface water availability, therefore

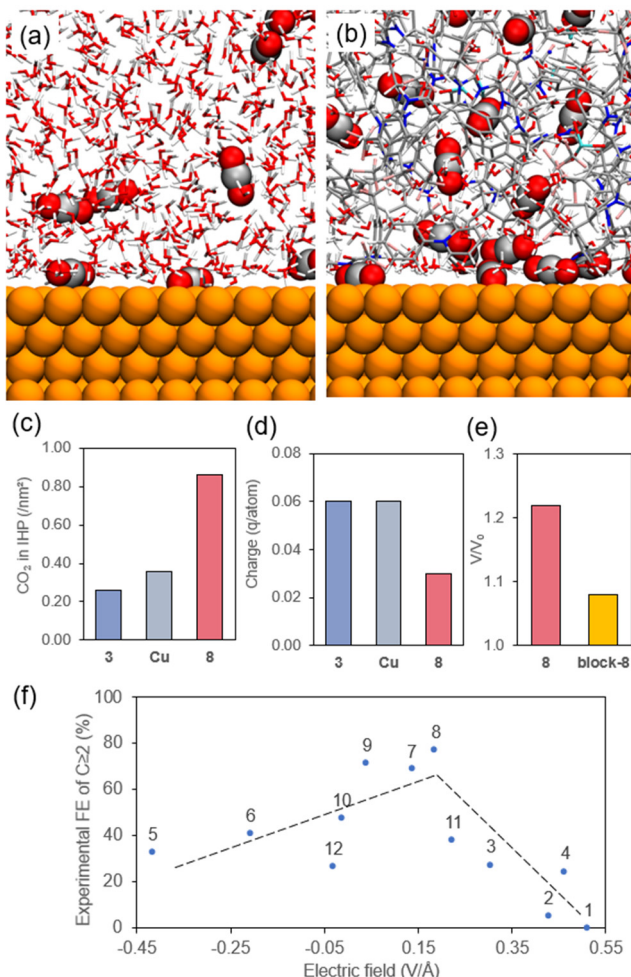


**Figure 8.** Interface structure after 12 ns molecular dynamics simulations: (a) water/Cu interface; (b) random copolymer 8 + water/Cu interface. Colors code: Cu, orange; C, gray; O, red; N, blue; F, pink; S, cyan; H, white. CO<sub>2</sub> molecules are highlighted for viewing convenience. (c) Comparison of local CO<sub>2</sub> concentrations among Cu (in gray), polymer 3 (in blue), and random copolymer 8 (in red). (d) Comparison of the surface charge per atom among Cu (in gray), polymer 3 (in blue), and random copolymer 8 (in red) from Qeq predictions.<sup>27</sup> (e) Comparison of the ratio of volume between random copolymer 8 (in red) and block copolymer block-8 (in yellow). (f) Relationship of the electric field (V/Å) from MD with the Faradaic efficiencies from the experiment. The dashed lines are shown for viewing convenience.

inhibiting the competing HER. For example, the average numbers of H<sub>2</sub>O molecules at the water/Cu interface are  $8.16 \pm 0.04/\text{nm}^2$ ,  $10.54 \pm 0.04/\text{nm}^2$ , and  $12.65 \pm 0.05/\text{nm}^2$  for random copolymer 8, polymer 3, and pure Cu, respectively. (For a complete comparison of the local CO<sub>2</sub> and H<sub>2</sub>O concentrations, see Figures S13 and S14 in the Supporting Information.) Additionally, the change in the H<sub>2</sub>O concentration is likely to influence the diffusion of ions during electrolysis. This could lead to an increase in the local pH on the catalyst surface, promoting C<sub>2+</sub> selectivity.

This increase in the local concentration of CO<sub>2</sub> is due to the microscopic hydrophobic effect in the first monolayer (ML) at the Cu surface. The solubility of CO<sub>2</sub> in water is low, so that a hydrophobic interface can help increase the surface concentration of CO<sub>2</sub>, which in turn enhances both CO<sub>2</sub> reduction to CO and the subsequent reduction of multiple CO molecules to

C<sub>2+</sub> products. This will lead to an increase in C<sub>2+</sub> product selectivity, because an increased surface coverage of \*CO is known to both promote CO dimerization and also weaken \*H adsorption that can inhibit the HER.<sup>24</sup> This microscopic hydrophobicity emphasizes the interaction of the polymer and CO<sub>2</sub> at the first ML and need not be related to the macroscopic hydrophobicity of the polymer film. The latter can be accurately measured experimentally but does not correlate well with CO<sub>2</sub> reduction to C<sub>2+</sub> products.<sup>12h</sup> Although it is more relevant to the CO<sub>2</sub> reaction, the microscopic hydrophobicity in the first ML is hard to determine from the experiment. Instead, the surface charge has been demonstrated to be an effective descriptor of microscopic hydrophobicity that can correlate with CO<sub>2</sub> reduction performance,<sup>12g,h</sup> because the charge distribution and produced electric field reflect the overall effect of the distribution of cations and anions. This specific distribution, in turn, determines the amount of electric charge stored in the double-layer capacitor that significantly affects the electrochemical reaction, because such an electric field regulates the orientation of water, either with OH pointing to the surface or not.<sup>26</sup> The UFF force field uses the Qeq method<sup>27</sup> to calculate the charge, which has been validated to reproduce QM charges.<sup>28</sup> Figure 8d shows the comparisons of surface charges for water/Cu and random copolymer 8 + water/Cu. We see that the surface charge of water/Cu (per atom) is +0.06 and that of polymer 3 + water/Cu is +0.06, while that of polymer 8 + water/Cu is +0.03. These simulation results suggest that random copolymer 8 + water/Cu leads to improved microscopic hydrophobicity in comparison to water/Cu, explaining why it increases the local concentration of CO<sub>2</sub> in the IHP.

In addition, the porosity of the polymer is expected to be important for mass transport.<sup>29</sup> The experimental results show that the selectivity of the CO<sub>2</sub>RR for the random copolymer 8 is better than that of the block copolymer block-8. In order to understand these experimental results, we compared a simulation model of block-8 with random copolymer 8. We find that block-8 is more ordered and less porous than random copolymer 8. This decrease in porosity should decrease the mass transfer of reactants, especially CO<sub>2</sub>, explaining the worse CO<sub>2</sub> reduction performance of block-8. To quantify the structure difference between random copolymer 8 and block-8, we compared the ratio between the effective volume of the polymer at the electrode (V) with that of just the polymer (V<sub>0</sub>). A larger V/V<sub>0</sub> indicates increased porosity, which should lead to increased CO<sub>2</sub> reduction. As shown in Figure 8e, the random copolymer 8 has V/V<sub>0</sub> 13% larger porosity in comparison to block-8, explaining the experimental observation. This suggests the permeability of CO<sub>2</sub> gas is important in polymer design.

The above effects also influence the induced electric field at the interface. The electric field, arising from both the surface charge and the charge distribution, has been demonstrated as an effective descriptor for CO<sub>2</sub> reduction.<sup>19b</sup> As shown in Figure 8f, we found that the CO<sub>2</sub> reduction performance correlates with electric field strength, leading to a volcano curve, with random copolymers 7–9 located close to the peak. This explains the enhanced performance of these polymers, suggesting that the surface electric field intensity may be a useful descriptor for *in silico* discovery of improved polymer materials for CO<sub>2</sub> reduction, especially for such complex systems as polymer-modified heterogeneous electrocatalysis

interfaces. Due to the complexity of the system, linear regression, taking into account all possible descriptors, might be a good way to correlate the experimental results with the interface structure as revealed from the MD simulations. Although the current data set is too limited for regression analysis, we will consider gathering more data, either from experiment or by augmentation from simulations, to facilitate a robust prediction model in the future.

## CONCLUSION

In summary, a new strategy for enhancing the selectivity for the CO<sub>2</sub>RR using a heterogeneous Cu catalyst was realized by employing a series of random copolymers as the surface modifier. A unique tricomponent copolymer was identified to provide optimal Faradaic efficiencies of ethylene (55%) and C<sub>2+</sub> products (77%). A surface characterization indicates the robustness of the film under CO<sub>2</sub>RR conditions, which is enabled by the incorporation of a phenylpyridinium component. Nanostructuring effects and electronic effects were ruled out by AFM, SEM, and XPS studies. A further MD simulation demonstrated that the presence of the optimal polymer modifier increases the local CO<sub>2</sub> concentration. In comparison with the corresponding block copolymer, the random copolymer is more porous, allowing access and mass transport of the reactants. In addition, the interfacial electric field plays an important role in performance enhancement. Future efforts will focus on employing this strategy on nanostructured Cu catalyst and gas-diffusion electrodes.<sup>30</sup>

## EXPERIMENTAL SECTION

**Electrode Preparation.** The surface preparation of Cu prior to each experiment consisted of mechanical polishing (1600 sandpaper, 3M) until no discoloration was visible and then electropolishing in phosphoric acid potentiostatically at 2.1 V for 40 min versus a graphite foil (0.13 mm thick, Alfa Aesar, 99.8% metals basis) counter electrode placed at a distance of ~1.5 cm. The Cu foil was subsequently washed with ultrapure water and dried under a stream of nitrogen gas. A methanol solution of the polymer (300 μL, 5 mg/mL) was dropped onto the electropolished Cu, which was rotated at 3000 rpm for 60 s by using a LAURELL WS-400BZ-6NPP/LITE spin coater. After deposition by spin coating, the electrode was further annealed at 70 °C for 10 min.

**Chronoamperometry (CA).** CA experiments were conducted in the cell with a CO<sub>2</sub> flow rate of 5 sccm using a Biologic potentiostat (VSP-300). Prior to CA experiments, linear scan voltammetry was conducted from the open circuit potential to -1.05 V vs RHE at a scan rate of 20 mV/s in order to reduce any oxidized Cu. The impedance was then measured, and a correction for the ohmic resistance was applied to the CA experiment. Each trial was run at -1.08 V vs RHE for 64 min. The outlet of the electrochemical cell was connected to an in-line gas chromatograph (GC), and the gaseous products were injected into the chromatograph every 4.2 min. At the end of the experiment, the liquid from both the cathode and the anode was analyzed via <sup>1</sup>H NMR spectroscopy to quantify the amounts of formic acid, ethanol, and *n*-propanol. The product selectivity and activities are reported in terms of Faradaic efficiencies (FE) and total current densities (mA/cm<sup>2</sup>). The Faradaic efficiency of a specific product was calculated as the ratio between the moles of a product produced by the electrode and the equivalents of electrons passed through the electrode. All potentials were converted from the Ag/AgCl scale to the reversible hydrogen electrode (RHE) scale by using  $E_{\text{RHE}} = E_{\text{Ag/AgCl}} - 0.197 - 0.059 \times \text{pH}$ , where  $E_{\text{RHE}}$ ,  $E_{\text{Ag/AgCl}}$ , and pH are the potential vs RHE, the measured potential vs the Ag/AgCl reference electrode, and pH of the electrolyte (6.8).

**Atomic Simulation.** Density functional theory (DFT) calculations were carried out by using the Vienna Ab initio Simulation

Package (VASP), version 5.4.4.<sup>31</sup> DFT calculations include an optimization of fragments of the polymer interacting with Cu (111) surface. The optimized geometries and binding energies were obtained to train and validate the force field. Molecular mechanics (MM) calculations were carried out by using the large-scale atomic/molecular massively parallel simulator (LAMMPS), version 12Dec20.<sup>32</sup> In the MM calculations, H<sub>2</sub>O, CO<sub>2</sub>, polymers, anions, and Cu metal were described by the universal force field (UFF)<sup>25</sup> with vdW terms revised to reproduce DFT calculations. More details about the simulations are given in the Supporting Information.

## ASSOCIATED CONTENT

### Supporting Information

The Supporting Information is available free of charge at <https://pubs.acs.org/doi/10.1021/jacs.0c12478>.

Materials, instruments, synthesis procedure and characterization data of monomers and copolymers, XPS study, contact angle measurements, and details of the atomic simulation ([PDF](#))

## AUTHOR INFORMATION

### Corresponding Authors

William A. Goddard III – Joint Center for Artificial Photosynthesis and Materials and Process Simulation Center, California Institute of Technology, Pasadena, California 91125, United States;  [orcid.org/0000-0003-0097-5716](https://orcid.org/0000-0003-0097-5716); Email: [wag@caltech.edu](mailto:wag@caltech.edu)

Robert H. Grubbs – Joint Center for Artificial Photosynthesis and The Arnold and Mabel Beckman Laboratory of Chemical Synthesis, Division of Chemistry and Chemical Engineering, California Institute of Technology, Pasadena, California 91125, United States;  [orcid.org/0000-0002-0057-7817](https://orcid.org/0000-0002-0057-7817); Email: [rhg@caltech.edu](mailto:rhg@caltech.edu)

### Authors

Jianchun Wang – Joint Center for Artificial Photosynthesis and The Arnold and Mabel Beckman Laboratory of Chemical Synthesis, Division of Chemistry and Chemical Engineering, California Institute of Technology, Pasadena, California 91125, United States

Tao Cheng – Joint Center for Artificial Photosynthesis and Materials and Process Simulation Center, California Institute of Technology, Pasadena, California 91125, United States

Aidan Q. Fenwick – Joint Center for Artificial Photosynthesis, California Institute of Technology, Pasadena, California 91125, United States

Turki N. Baroud – Department of Mechanical Engineering, King Fahd University of Petroleum and Mineral, Dhahran 31261, Saudi Arabia;  [orcid.org/0000-0001-6430-9128](https://orcid.org/0000-0001-6430-9128)

Alonso Rosas-Hernández – Joint Center for Artificial Photosynthesis, California Institute of Technology, Pasadena, California 91125, United States

Jeong Hoon Ko – The Arnold and Mabel Beckman Laboratory of Chemical Synthesis, Division of Chemistry and Chemical Engineering, California Institute of Technology, Pasadena, California 91125, United States;  [orcid.org/0000-0003-2000-3789](https://orcid.org/0000-0003-2000-3789)

Quan Gan – The Arnold and Mabel Beckman Laboratory of Chemical Synthesis, Division of Chemistry and Chemical Engineering, California Institute of Technology, Pasadena, California 91125, United States

Complete contact information is available at:  
<https://pubs.acs.org/doi/10.1021/jacs.0c12478>

## Funding

This study was supported by the King Fahd University of Petroleum and Minerals (R.H.G.) and the Joint Center for Artificial Photosynthesis, a Department of Energy (DOE) Energy Innovation Hub, supported through the Office of Science of the U.S. Department of Energy under Award Number DE-SC0004993.

## Notes

The authors declare no competing financial interest.

## ACKNOWLEDGMENTS

This research benefited from the use of instrumentation made available by the Caltech CCE Multiuser Mass Spectrometry Laboratory. XPS data were collected at the Molecular Materials Research Center in the Beckman Institute of the California Institute of Technology. Nick Watkins is thanked for assistance with SEM experiments. Dr. Shunsuke Sato, Dr. Brendon J. McNicholas, and Dr. Yan Xu are thanked for their discussions.

## REFERENCES

- (1) (a) Nitopi, S.; Bertheussen, E.; Scott, S. B.; Liu, X. Y.; Engstfeld, A. K.; Horch, S.; Seger, B.; Stephens, I. E. L.; Chan, K.; Hahn, C.; Norskov, J. K.; Jaramillo, T. F.; Chorkendorff, I. Progress and Perspectives of Electrochemical CO<sub>2</sub> Reduction on Copper in Aqueous Electrolyte. *Chem. Rev.* **2019**, *119*, 7610–7672. (b) Kibria, M. G.; Edwards, J. P.; Gabardo, C. M.; Dinh, C. T.; Seifitokaldani, A.; Sinton, D.; Sargent, E. H. Electrochemical CO<sub>2</sub> Reduction into Chemical Feedstocks: From Mechanistic Electrocatalysis Models to System Design. *Adv. Mater.* **2019**, *31*, 1807166.
- (2) (a) Hori, Y.; Kikuchi, K.; Suzuki, S. Production of CO and CH<sub>4</sub> in Electrochemical Reduction of CO<sub>2</sub> at Metal Electrodes in Aqueous Hydrogencarbonate Solution. *Chem. Lett.* **1985**, *14*, 1695–1698. (b) Hori, Y.; Kikuchi, K.; Murata, A.; Suzuki, S. Production of Methane and Ethylene in Electrochemical Reduction of Carbon-Dioxide at Copper Electrode in Aqueous Hydrogencarbonate Solution. *Chem. Lett.* **1986**, *15*, 897–898. (c) Kuhl, K. P.; Cave, E. R.; Abram, D. N.; Jaramillo, T. F. New Insights into the Electrochemical Reduction of Carbon Dioxide on Metallic Copper Surfaces. *Energy Environ. Sci.* **2012**, *5*, 7050–7059.
- (3) (a) Li, C. W.; Kanan, M. W. CO<sub>2</sub> Reduction at Low Overpotential on Cu Electrodes Resulting from the Reduction of Thick Cu<sub>2</sub>O Films. *J. Am. Chem. Soc.* **2012**, *134*, 7231–4. (b) Li, C. W.; Ciston, J.; Kanan, M. W. Electroreduction of Carbon Monoxide to Liquid Fuel on Oxide-derived Nanocrystalline Copper. *Nature* **2014**, *508*, 504–507. (c) Verdaguera-Casadevall, A.; Li, C. W.; Johansson, T. P.; Scott, S. B.; McKeown, J. T.; Kumar, M.; Stephens, I. E.; Kanan, M. W.; Chorkendorff, I. Probing the Active Surface Sites for CO Reduction on Oxide-Derived Copper Electrocatalysts. *J. Am. Chem. Soc.* **2015**, *137*, 9808–11. (d) Feng, X.; Jiang, K.; Fan, S.; Kanan, M. W. A Direct Grain-Boundary-Activity Correlation for CO Electroreduction on Cu Nanoparticles. *ACS Cent. Sci.* **2016**, *2*, 169–74. (e) Mariano, R. G.; McKelvey, K.; White, H. S.; Kanan, M. W. Selective Increase in CO<sub>2</sub> Electroreduction Activity at Grain-boundary Surface Terminations. *Science* **2017**, *358*, 1187–1192.
- (4) (a) Mistry, H.; Varela, A. S.; Bonifacio, C. S.; Zegkinoglou, I.; Sinev, I.; Choi, Y. W.; Kisslinger, K.; Stach, E. A.; Yang, J. C.; Strasser, P.; Roldan Cuenya, B. Highly Selective Plasma-Activated Copper Catalysts for Carbon Dioxide Reduction to Ethylene. *Nat. Commun.* **2016**, *7*, 12123. (b) Eilert, A.; Cavalca, F.; Roberts, F. S.; Osterwalder, J.; Liu, C.; Favaro, M.; Crumlin, E. J.; Ogasawara, H.; Friebel, D.; Pettersson, L. G.; Nilsson, A. Subsurface Oxygen in Oxide-Derived Copper Electrocatalysts for Carbon Dioxide Reduction. *J. Phys. Chem. Lett.* **2017**, *8*, 285–290. (c) Xiao, H.; Goddard, W. A., III; Cheng, T.; Liu, Y. Cu Metal Embedded in Oxidized Matrix Catalyst to Promote CO<sub>2</sub> Activation and CO Dimerization for Electrochemical Reduction of CO<sub>2</sub>. *Proc. Natl. Acad. Sci. U.S.A.* **2017**, *114*, 6685–6688.
- (5) Zhou, Y.; Che, F.; Liu, M.; Zou, C.; Liang, Z.; De Luna, P.; Yuan, H.; Li, J.; Wang, Z.; Xie, H.; Li, H.; Chen, P.; Bladt, E.; Quintero-Bermudez, R.; Sham, T. K.; Bals, S.; Hofkens, J.; Sinton, D.; Chen, G.; Sargent, E. H. Dopant-induced Electron Localization Drives CO<sub>2</sub> Reduction to C<sub>2</sub> Hydrocarbons. *Nat. Chem.* **2018**, *10*, 974–980.
- (6) (a) Roberts, F. S.; Kuhl, K. P.; Nilsson, A. High Selectivity for Ethylene from Carbon Dioxide Reduction over Copper Nanocube Electrocatalysts. *Angew. Chem., Int. Ed.* **2015**, *54*, 5179–5182. (b) Jiang, K.; Sandberg, R. B.; Akey, A. J.; Liu, X. Y.; Bell, D. C.; Norskov, J. K.; Chan, K. R.; Wang, H. T. Metal Ion Cycling of Cu Foil for Selective C-C Coupling in Electrochemical CO<sub>2</sub> Reduction. *Nat. Catal.* **2018**, *1*, 111–119.
- (7) Yang, K. D.; Ko, W. R.; Lee, J. H.; Kim, S. J.; Lee, H.; Lee, M. H.; Nam, K. T. Morphology-Directed Selective Production of Ethylene or Ethane from CO<sub>2</sub> on a Cu Mesopore Electrode. *Angew. Chem., Int. Ed.* **2017**, *56*, 796–800.
- (8) Li, Y.; Kim, D.; Louisia, S.; Xie, C.; Kong, Q.; Yu, S.; Lin, T.; Aloni, S.; Fakra, S. C.; Yang, P. Electrochemically Scrambled Nanocrystals are Catalytically Active for CO<sub>2</sub>-to-Multicarbons. *Proc. Natl. Acad. Sci. U. S. A.* **2020**, *117*, 9194–9201.
- (9) Francke, R.; Schille, B.; Roemelt, M. Homogeneously Catalyzed Electroreduction of Carbon Dioxide-Methods, Mechanisms, and Catalysts. *Chem. Rev.* **2018**, *118*, 4631–4701.
- (10) (a) Beley, M.; Collin, J.-P.; Ruppert, R.; Sauvage, J.-P. Nickel(II)-cyclam: An Extremely Selective Electrocatalyst for Reduction of CO<sub>2</sub> in Water. *J. Chem. Soc., Chem. Commun.* **1984**, 1315–1316. (b) Costentin, C.; Drouet, S.; Robert, M.; Savéant, J.-M. A Local Proton Source Enhances CO<sub>2</sub> Electroreduction to CO by a Molecular Fe Catalyst. *Science* **2012**, *338*, 90–94. (c) Agarwal, J.; Shaw, T. W.; Schaefer, H. F., 3rd; Bocarsly, A. B. Design of a Catalytic Active Site for Electrochemical CO<sub>2</sub> Reduction with Mn(I)-Tricarbonyl Species. *Inorg. Chem.* **2015**, *54*, 5285–94. (d) Azcarate, I.; Costentin, C.; Robert, M.; Saveant, J. M. Through-Space Charge Interaction Substituent Effects in Molecular Catalysis Leading to the Design of the Most Efficient Catalyst of CO<sub>2</sub>-to-CO Electrochemical Conversion. *J. Am. Chem. Soc.* **2016**, *138*, 16639–16644. (e) Ngo, K. T.; McKinnon, M.; Mahanti, B.; Narayanan, R.; Grills, D. C.; Ertem, M. Z.; Rochford, J. Turning on the Protonation-First Pathway for Electrocatalytic CO<sub>2</sub> Reduction by Manganese Bipyridyl Tricarbonyl Complexes. *J. Am. Chem. Soc.* **2017**, *139*, 2604–2618. (f) Nichols, E. M.; Derrick, J. S.; Nistanaki, S. K.; Smith, P. T.; Chang, C. J. Positional Effects of Second-sphere Amide Pendants on Electrochemical CO<sub>2</sub> Reduction Catalyzed by Iron Porphyrins. *Chem. Sci.* **2018**, *9*, 2952–2960. (g) Sung, S.; Li, X. H.; Wolf, L. M.; Meeder, J. R.; Bhuvanesh, N. S.; Grice, K. A.; Panetier, J. A.; Nippe, M. Synergistic Effects of Imidazolium-Functionalization on fac-Mn(CO)<sub>3</sub> Bipyridine Catalyst Platforms for Electrocatalytic Carbon Dioxide Reduction. *J. Am. Chem. Soc.* **2019**, *141*, 6569–6582.
- (11) Nam, D. H.; De Luna, P.; Rosas-Hernandez, A.; Thevenon, A.; Li, F.; Agapie, T.; Peters, J. C.; Shekhah, O.; Eddaoudi, M.; Sargent, E. H. Molecular Enhancement of Heterogeneous CO<sub>2</sub> Reduction. *Nat. Mater.* **2020**, *19*, 266–276.
- (12) (a) Kim, C.; Jeon, H. S.; Eom, T.; Jee, M. S.; Kim, H.; Friend, C. M.; Min, B. K.; Hwang, Y. J. Achieving Selective and Efficient Electrocatalytic Activity for CO<sub>2</sub> Reduction Using Immobilized Silver Nanoparticles. *J. Am. Chem. Soc.* **2015**, *137*, 13844–50. (b) Zhao, Y.; Wang, C.; Liu, Y.; MacFarlane, D. R.; Wallace, G. G. Engineering Surface Amine Modifiers of Ultrasmall Gold Nanoparticles Supported on Reduced Graphene Oxide for Improved Electrochemical CO<sub>2</sub> Reduction. *Adv. Energy Mater.* **2018**, *8*, 1801400. (c) Cao, Z.; Derrick, J. S.; Xu, J.; Gao, R.; Gong, M.; Nichols, E. M.; Smith, P. T.; Liu, X.; Wen, X.; Coperet, C.; Chang, C. J. Chelating N-Heterocyclic Carbene Ligands Enable Tuning of Electrocatalytic CO<sub>2</sub> Reduction to Formate and Carbon Monoxide: Surface Organometallic Chemistry. *Angew. Chem., Int. Ed.* **2018**, *57*, 4981–4985. (d) Fang, Y.; Flake, J. C. Electrochemical Reduction of CO<sub>2</sub> at Functionalized Au Electrodes. *J. Am. Chem. Soc.* **2017**, *139*, 3399–3405. (e) Xie, M. S.; Xia, B. Y.; Li, Y.; Yan, Y.; Yang, Y.; Sun, Q.; Chan, S. H.; Fisher, A.; Wang, X. Amino Acid Modified Copper Electrodes for the Enhanced Selective

- Electroreduction of Carbon Dioxide towards Hydrocarbons. *Energy Environ. Sci.* **2016**, *9*, 1687–1695. (f) Han, Z.; Kortlever, R.; Chen, H.-Y.; Peters, J. C.; Agapie, T. CO<sub>2</sub> Reduction Selective for C ≥ 2 Products on Polycrystalline Copper with N-Substituted Pyridinium Additives. *ACS Cent. Sci.* **2017**, *3*, 853–859. (g) Li, F.; Thevenon, A.; Rosas-Hernández, A.; Wang, Z.; Li, Y.; Gabardo, C. M.; Ozden, A.; Dinh, C. T.; Li, J.; Wang, Y.; Edwards, J. P.; Xu, Y.; McCallum, C.; Tao, L.; Liang, Z. Q.; Luo, M.; Wang, X.; Li, H.; O'Brien, C. P.; Tan, C. S.; Nam, D. H.; Quintero-Bermudez, R.; Zhuang, T. T.; Li, Y. C.; Han, Z.; Britt, R. D.; Sinton, D.; Agapie, T.; Peters, J. C.; Sargent, E. H. Molecular Tuning of CO<sub>2</sub>-to-Ethylene Conversion. *Nature* **2020**, *577*, 509–513. (h) Buckley, A. K.; Lee, M.; Cheng, T.; Kazantsev, R. V.; Larson, D. M.; Goddard, W. A.; Toste, F. D.; Toma, F. M. Electrocatalysis at Organic-Metal Interfaces: Identification of Structure-Reactivity Relationships for CO<sub>2</sub> Reduction at Modified Cu Surfaces. *J. Am. Chem. Soc.* **2019**, *141*, 7355–7364. (i) Ahn, S.; Klyukin, K.; Wakeham, R. J.; Rudd, J. A.; Lewis, A. R.; Alexander, S.; Carla, F.; Alexandrov, V.; Andreoli, E. Poly-Amide Modified Copper Foam Electrodes for Enhanced Electrochemical Reduction of Carbon Dioxide. *ACS Catal.* **2018**, *8*, 4132–4142. (j) Wei, X.; Yin, Z.; Lyu, K.; Li, Z.; Gong, J.; Wang, G.; Xiao, L.; Lu, J.; Zhuang, L. Highly Selective Reduction of CO<sub>2</sub> to C<sub>2+</sub> Hydrocarbons at Copper/Polyaniline Interfaces. *ACS Catal.* **2020**, *10*, 4103–4111.
- (13) Ovalle, V. J.; Waegele, M. M. Understanding the Impact of N-Arylpyridinium Ions on the Selectivity of CO<sub>2</sub> Reduction at the Cu/Electrolyte Interface. *J. Phys. Chem. C* **2019**, *123*, 24453–24460.
- (14) Thevenon, A.; Rosas-Hernández, A.; Peters, J. C.; Agapie, T. In-Situ Nanostructuring and Stabilization of Polycrystalline Copper by an Organic Salt Additive Promotes Electrocatalytic CO<sub>2</sub> Reduction to Ethylene. *Angew. Chem., Int. Ed.* **2019**, *58*, 16952–16958.
- (15) (a) Bielawski, C. W.; Grubbs, R. H. Living Ring-Opening Metathesis Polymerization. *Prog. Polym. Sci.* **2007**, *32*, 1–29. (b) Nguyen, S. T.; Johnson, L. K.; Grubbs, R. H.; Ziller, J. W. Ring-Opening Metathesis Polymerization (ROMP) of Norbornene by a Group VIII Carbene Complex in Protic Media. *J. Am. Chem. Soc.* **1992**, *114*, 3974–3975.
- (16) Wagner, A.; Sahm, C. D.; Reisner, E. Towards Molecular Understanding of Local Chemical Environment Effects in Electro- and Photocatalytic CO<sub>2</sub> Reduction. *Nat. Catal.* **2020**, *3*, 775–786.
- (17) (a) Murata, A.; Hori, Y. Product Selectivity Affected by Cationic Species in Electrochemical Reduction of CO<sub>2</sub> and CO at a Cu Electrode. *Bull. Chem. Soc. Jpn.* **1991**, *64*, 123–127. (b) Singh, M. R.; Kwon, Y.; Lum, Y.; Ager, J. W.; Bell, A. T. Hydrolysis of Electrolyte Cations Enhances the Electrochemical Reduction of CO<sub>2</sub> over Ag and Cu. *J. Am. Chem. Soc.* **2016**, *138*, 13006–13012. (c) Resasco, J.; Chen, L. D.; Clark, E.; Tsai, C.; Hahn, C.; Jaramillo, T. F.; Chan, K.; Bell, A. T. Promoter Effects of Alkali Metal Cations on the Electrochemical Reduction of Carbon Dioxide. *J. Am. Chem. Soc.* **2017**, *139*, 11277–11287. (d) Gunathunge, C. M.; Ovalle, V. J.; Waegele, M. M. Probing Promoting Effects of Alkali Cations on the Reduction of CO at the Aqueous Electrolyte/Copper Interface. *Phys. Chem. Chem. Phys.* **2017**, *19*, 30166–30172. (e) Ringe, S.; Clark, E. L.; Resasco, J.; Walton, A.; Seger, B.; Bell, A. T.; Chan, K. Understanding Cation Effects in Electrochemical CO<sub>2</sub> Reduction. *Energy Environ. Sci.* **2019**, *12*, 3001–3014.
- (18) Rosen, B. A.; Salehi-Khojin, A.; Thorson, M. R.; Zhu, W.; Whipple, D. T.; Kenis, P. J. A.; Masel, R. I. Ionic Liquid-Mediated Selective Conversion of CO<sub>2</sub> to CO at Low Overpotentials. *Science* **2011**, *334*, 643–644.
- (19) (a) Rosen, B. A.; Haan, J. L.; Mukherjee, P.; Braunschweig, B.; Zhu, W.; Salehi-Khojin, A.; Dlott, D. D.; Masel, R. I. In Situ Spectroscopic Examination of a Low Overpotential Pathway for Carbon Dioxide Conversion to Carbon Monoxide. *J. Phys. Chem. C* **2012**, *116*, 15307–15312. (b) Chen, L. D.; Urushihara, M.; Chan, K.; Nørskov, J. K. Electric Field Effects in Electrochemical CO<sub>2</sub> Reduction. *ACS Catal.* **2016**, *6*, 7133–7139. (c) Feaster, J. T.; Jongerius, A. L.; Liu, X.; Urushihara, M.; Nitopi, S. A.; Hahn, C.; Chan, K.; Nørskov, J. K.; Jaramillo, T. F. Understanding the Influence of [EMIM]Cl on the Suppression of the Hydrogen Evolution Reaction on Transition Metal Electrodes. *Langmuir* **2017**, *33*, 9464–9471.
- (20) Hugar, K. M.; Kostalik, H. A.; Coates, G. W. Imidazolium Cations with Exceptional Alkaline Stability: A Systematic Study of Structure-Stability Relationships. *J. Am. Chem. Soc.* **2015**, *137*, 8730–8737.
- (21) Nichols, E. M.; Chang, C. J. Urea-Based Multipoint Hydrogen-Bond Donor Additive Promotes Electrochemical CO<sub>2</sub> Reduction Catalyzed by Nickel Cyclam. *Organometallics* **2019**, *38*, 1213–1218.
- (22) Haviv, E.; Azaiza-Dabbah, D.; Carmeli, R.; Avram, L.; Martin, J. M. L.; Neumann, R. A Thiourea Tether in the Second Coordination Sphere as a Binding Site for CO<sub>2</sub> and a Proton Donor Promotes the Electrochemical Reduction of CO<sub>2</sub> to CO Catalyzed by a Rhodium Bipyridine-Type Complex. *J. Am. Chem. Soc.* **2018**, *140*, 12451–12456.
- (23) Tang, W.; Peterson, A. A.; Varela, A. S.; Jovanov, Z. P.; Bech, L.; Durand, W. J.; Dahl, S.; Norskov, J. K.; Chorkendorff, I. The Importance of Surface Morphology in Controlling the Selectivity of Polycrystalline Copper for CO<sub>2</sub> Electroreduction. *Phys. Chem. Chem. Phys.* **2012**, *14*, 76–81.
- (24) Tan, Y. C.; Lee, K. B.; Song, H.; Oh, J. Modulating Local CO<sub>2</sub> Concentration as a General Strategy for Enhancing C-C Coupling in CO<sub>2</sub> Electroreduction. *Joule* **2020**, *4*, 1104–1120.
- (25) Rappé, A. K.; Casewit, C. J.; Colwell, K.; Goddard, W. A., III; Skiff, W. M. UFF, a Full Periodic Table Force Field for Molecular Mechanics and Molecular Dynamics Simulations. *J. Am. Chem. Soc.* **1992**, *114*, 10024–10035.
- (26) Cheng, T.; Wang, L.; Merinov, B. V.; Goddard, W. A. Explanation of Dramatic pH-Dependence of Hydrogen Binding on Noble Metal Electrode: Greatly Weakened Water Adsorption at High pH. *J. Am. Chem. Soc.* **2018**, *140*, 7787–7790.
- (27) Rappe, A. K.; Goddard III, W. A. Charge Equilibration for Molecular Dynamics Simulations. *J. Phys. Chem.* **1991**, *95*, 3358–3363.
- (28) Naserifar, S.; Brooks, D. J.; Goddard III, W. A.; Cvicet, V. Polarizable Charge Equilibration Model for Predicting Accurate Electrostatic Interactions in Molecules and Solids. *J. Chem. Phys.* **2017**, *146*, 124117.
- (29) Soniat, M.; Tesfaye, M.; Brooks, D.; Merinov, B.; Goddard III, W. A.; Weber, A. Z.; Houle, F. A Predictive Simulation of Non-steady-state Transport of Gases through Rubbery Polymer Membranes. *Polymer* **2018**, *134*, 125–142.
- (30) Dinh, C. T.; Burdyny, T.; Kibria, M. G.; Seifitokaldani, A.; Gabardo, C. M.; de Arquer, F. P. G.; Kiani, A.; Edwards, J. P.; De Luna, P.; Bushuyev, O. S.; Zou, C. Q.; Quintero-Bermudez, R.; Pang, Y. J.; Sinton, D.; Sargent, E. H. CO<sub>2</sub> Electroreduction to Ethylene via Hydroxide-Mediated Copper Catalysis at an Abrupt Interface. *Science* **2018**, *360*, 783–787.
- (31) Kresse, G.; Hafner, J. Ab Initio Molecular Dynamics for Liquid Metals. *Phys. Rev. B: Condens. Matter Mater. Phys.* **1993**, *47*, 558–561.
- (32) Plimpton, S. Fast Parallel Algorithms for Short-Range Molecular Dynamics. *J. Comput. Phys.* **1995**, *117*, 1–19.